ACS NANO

www.acsnano.org

ARTICLE

Avoided Level Crossing and Entangled States of Interacting Hydrogen Molecules Detected by the Quantum Superposition Microscope

Yunpeng Xia, Likun Wang, Dan Bai, and Wilson Ho*

Cite This: *ACS Nano* 2023, 17, 23144–23151

Read Online

ACCESS | Metrics & More | Article Recommendations | Supporting Information

ABSTRACT: **Pump–probe measurements by ultrashort THz pulses can be used to excite and follow the coherence dynamics in the time domain of single hydrogen molecules (H_2) in the junction of a scanning tunneling microscope (STM). By tailoring the resonance frequency through the sample bias, we identified two spectral signatures of the interactions among multiple H_2 molecules. First, the avoided level crossing featured by energy gaps ranging from 20 to 80 GHz was observed because of the level repulsion between two H_2 molecules. Second, the tip can sense the signal of H_2 outside the junction through the projective measurement on the H_2 inside the junction, owing to the entangled states created through the interactions. A dipolar-type interaction was integrated into the tunneling two-level system model of H_2, enabling accurate reproduction of the observed behaviors. Our results obtained by the quantum superposition microscope reveal the intricate quantum mechanical interplay among H_2 molecules and additionally provide a 2D platform to investigate unresolved questions of amorphous materials.**

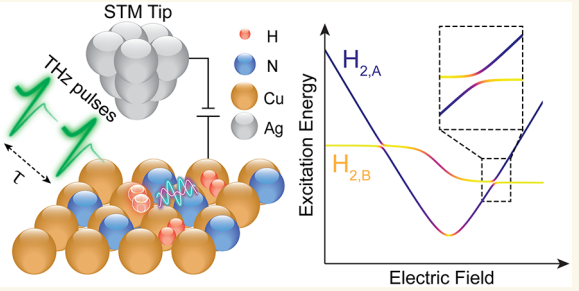

KEYWORDS: *quantum superposition microscope, broadband ultrafast terahertz scanning tunneling microscope, interacting two-level single molecules, avoided level crossing, superposition, entanglement*

A quantum entity that can oscillate between two nondegenerate states by quantum tunneling through a potential-energy barrier is termed a tunneling two-level system (TLS). For decades, atomic-scale TLSs residing in amorphous solids or glasses, especially interactions among them, have attracted wide attention because of their theoretical significance and their practical applications. The assumed general existence of TLSs in the materials led to theoretical predictions of several anomalous features compared to their crystalline counterparts.[1−4] Furthermore, the ubiquitous interactions among the TLSs implemented by superconducting qubits underlie the chief cause of decoherence and impediment to the advancement of quantum computing and other technologies that require long coherence time.[5,6] While TLSs present well-defined models for theoretical studies, their microscopic structures are generally unknown, and a detailed understanding of the interactions among them remains elusive. However, recent advances in superconducting qubit spectroscopy have examined the intriguing properties of these TLSs.[7−12]

Physisorbed H_2 molecules, trapped in an scanning tunneling microscope (STM) cavity, have been observed to display structural switching that manifests as the telegraph noise in the junction conductance.[13−15] A double-well TLS model has been developed based on this behavior, which could explain several other intriguing experimental observations, including the abnormally huge negative differential resistance[16,17] and the stochastic resonance.[14] Moreover, research has indicated that under cryogenic conditions H_2 molecules on a surface have a propensity to form clusters and nucleate around other molecules or metallic islands due to attractive van der Waals forces, to eventually develop phonon modes.[18−20] These findings suggest that physisorbed H_2 can serve as a model system for randomly distributed TLSs that interact with each other.

THz-STM has been proven as a powerful tool to investigate the atomic-scale dynamics with femtosecond temporal resolution owing to the ultrafast voltage transient induced by

Received: September 21, 2023
Revised: November 6, 2023
Accepted: November 8, 2023
Published: November 13, 2023

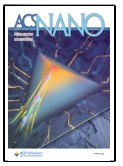

https://doi.org/10.1021/acsnano.3c09109
ACS Nano 2023, 17, 23144–23151

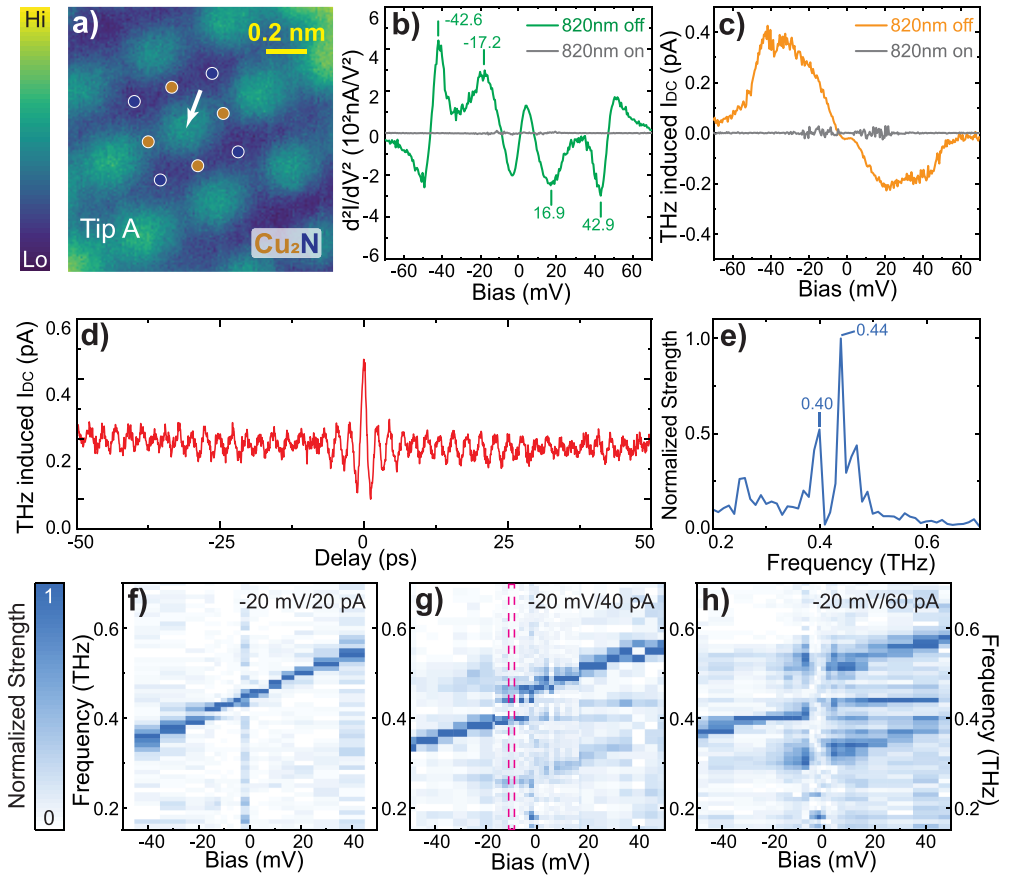

Figure 1. Spectroscopic signatures of two interacting H_2 molecules. (a) Constant current topographic image of a Cu_2N surface with a set point of −20 mV/40 pA; the superimposed brown and blue circles represent the positions of Cu and N atoms. (b) Spectrum by IETS and (c) spectrum by TIDCS were obtained at the same spot marked by the white arrow in (a) with the same set point of −20 mV/40 pA. Shining an 820 nm laser into the junction desorbs H_2 molecules, evidenced by the spectral features of the bare Cu_2N surface. (d) The pump−probe measurement of the THz-induced DC by the QSM, with tip bias ramped to −10 mV after turning off the feedback at the set point of −20 mV/40 pA. (e) Normalized fast Fourier transform (FFT) spectrum of (d) to highlight the resonance frequencies of H_2 in the junction. (f−h) Bias dependence of resonance frequencies of H_2. Each slice of the plot, such as the purple dashed box in (g), was taken from the normalized FFT spectrum (e) of the −50 to 50 ps delay scan spectrum (d). The feedback was turned off at the given set point [(f) −20 mV/20 pA; (g) −20 mV/40 pA; (h) −20 mV/60 pA], and the bias was then ramped to the corresponding value. For (g), the data were derived from −30 to 30 ps delay scan spectra, except for the bias range from −15 to 15 mV, where the delay scan spectra were from −50 to 50 ps.

THz pulses.[21−29] The voltage modulation across the STM junction introduced by THz pulses can respond to nonlinear $I-V$ characteristics and produce rectification or a DC current. In addition, a property of H_2 that sets it apart from other systems studied by THz-STM arises from the resonant transition between the two levels in H_2 induced by the absorption of THz photons.[27,29] By combining the pump−probe technique with the STM, we were able to reveal the resonance frequency of the TLS and further demonstrated that this frequency can be split from the interactions with the TLS of nearby H_2 molecules.

RESULTS AND DISCUSSION

Observation of Avoided Level Crossing. The quantum superposition microscope (QSM) incorporates the high sensitivity of the coherent superposition of two levels in a single molecule to its environment as the basis for atomic-scale spectroscopy and imaging. The setup of the QSM can be found in the Methods section and elsewhere.[27] The data were taken with H_2 saturated on the $Cu_2N/Cu(001)$ surface (Figure 1(a)). The chemical inhomogeneity of the Cu_2N surface can influence the TLS of H_2 trapped in the tip−surface cavity. Inelastic electron tunneling spectroscopy (IETS) (Figure 1(b)) and single-beam THz induced DC current spectroscopy (TIDCS) (Figure 1(c)) were performed over the hollow position of the Cu_2N island, indicated by the white arrow in Figure 1(a). Shining an 820 nm laser directly into the STM junction desorbs H_2 molecules from the surface, evidenced by spectra of the clean Cu_2N surface with IETS and TIDCS. The two structural states of H_2 have distinct conductance, and the transition between them can be facilitated through the excitation of vibrational (∼20 meV) and rotational (∼40 meV) modes of H_2 by tunneling electrons with sufficient energy, as revealed by IETS.[19,30,31] In addition to modulating the bias, THz pulses can resonantly induce the transition of the TLS for H_2 and alter the population of the two structural states. The difference between the spectra by IETS and TIDCS implies the THz-induced population change of the TLS. The underlying dynamics could be further revealed by the coherent oscillation of the THz-induced DC current (Figure 1(d)) from pump−probe measurements with time-delayed THz pulses. The oscillation frequencies correspond to the resonance frequencies of H_2 in the junction (Figure 1(e)) and exhibit a gap of 0.04 THz (40 GHz) centered at 0.42 THz. The two

https://doi.org/10.1021/acsnano.3c09109
ACS Nano 2023, 17, 23144−23151

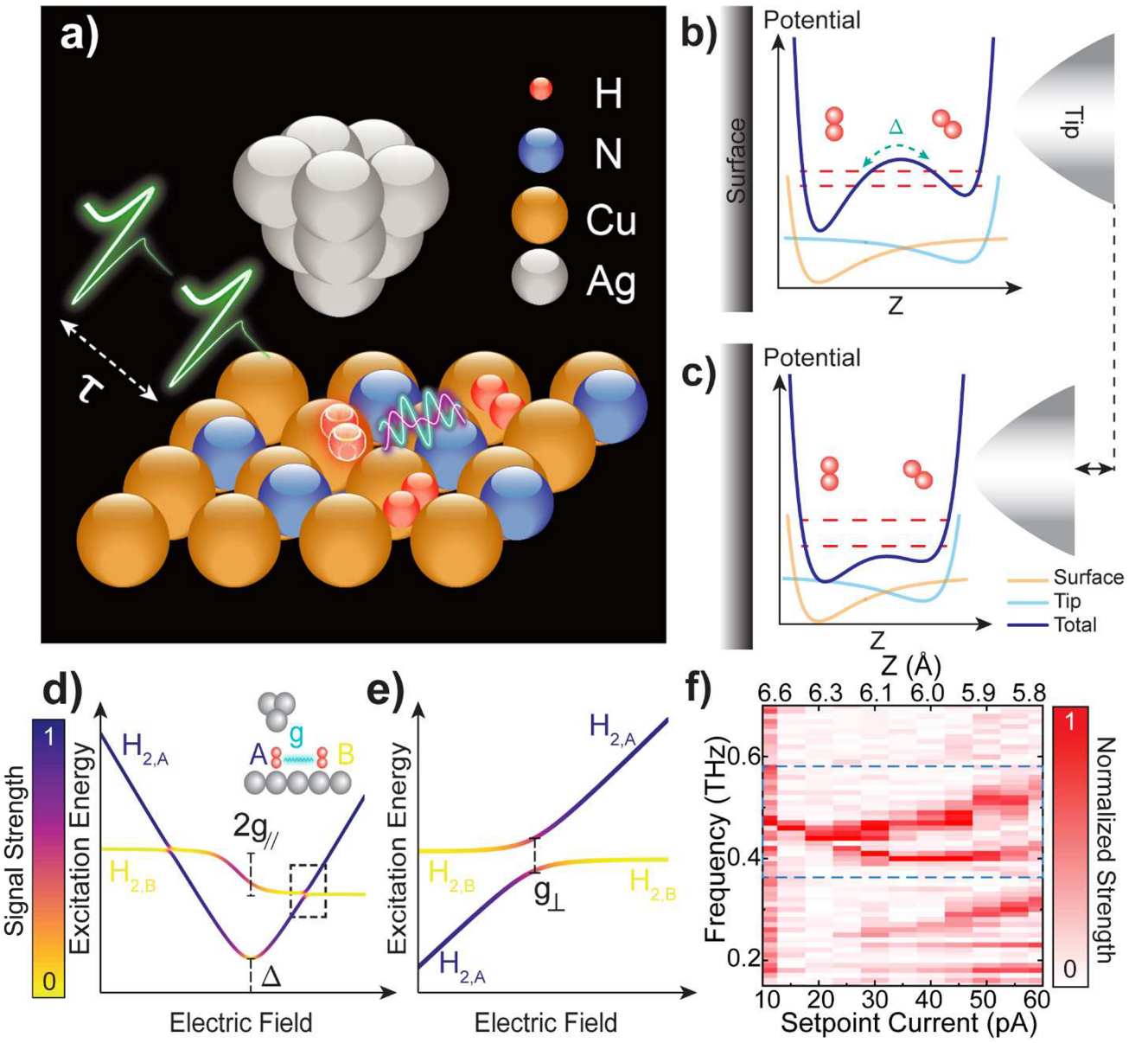

Figure 2. Avoided level crossing dependence on tip height. (a) Schematic diagram of the interacting H_2 molecules under THz irradiation on the Cu_2N surface. (b, c) Schematic illustration of the changes in the tilted double-well potential for different tip heights. (d) A typical excitation spectrum for the two interacting H_2 molecules. The color palette indicates the calculated absolute value of the population change of either structural state of the $H_{2,A}$, which is taken to be proportional to the signal strength. (e) The excitation spectrum which is zoomed into the avoided level crossing region indicated by the dashed box in (d). The meaning of parameters in (d) and (e) can be found in the SI. (f) Tip height (or the tunneling gap) dependence of the avoided level crossing gap enclosed by the blue dashed box. The height of the tip is controlled by the set point current since the set point bias was kept at −20 mV. After turning off the feedback, the bias was ramped to −5 mV, near the center of the avoided level crossing.

states of H_2 are expected to have different induced dipole moments, and by tuning the sample bias while maintaining the tip−surface distance, the energy spacing between the two states changed because of the Stark effect. Unlike prior observation of a complete energy branch,[27] a level repulsion was found from −20 to 0 mV (Figure 1(g)), and the gap size can be tailored by changing the tip−surface distance (Figure 1(f) and (h)). This phenomenon resembles the results from the Jaynes−Cummings model,[32] in which the tunnel junction could be viewed as an optical cavity. The TLS of H_2 interacts with the quantized photon mode of the junction, and the strength of such an interaction is inversely related to the size of the cavity, which is consistent with the observation that the size of the gap increases at a smaller junction. However, the center frequency of the gap, which reflects the energy of the cavity mode, exhibits no significant change, contradicting the fact that the energy of the cavity mode inversely changes with the size of the junction. In addition, the gap is centered around 0.4 THz (~1.7 meV), which eliminates the possibility of a coupling between the TLS of H_2 and the cavity mode or plasmonic field[33] whose energies are far above a few meVs.

Theoretical Model. It is generally believed that the phonon mode of the H_2 cluster is responsible for the IETS feature at approximately +(−)5 mV.[18−20] Through exchanging phonons, H_2 molecules can interact with each other, with the strength of interaction taking on a dipolar form of a/r^3.[34,35]

https://doi.org/10.1021/acsnano.3c09109
ACS Nano 2023, 17, 23144−23151

Here, a depicts the coupling between the H_2 and the strain field within the cluster and r is the distance between two interacting H_2 molecules. Since the physisorbed H_2 molecules are generally polarized and acquire permanent dipole moments due to substrate hybridization,[36] the intermolecular interaction should also have an electrical component. However, current experimental methods are not able to distinguish the two coupling mechanisms involving the strain field versus the dipole moment.

We, therefore, propose a model based on the dipolar-type interaction among H_2 molecules to explain the aforementioned behaviors.[8,37] For simplicity, only two H_2 molecules are included in the model, as shown in Figure 2(a). The Hamiltonian of this interacting system can be expressed as

$$H = \sum_{i=A,B} \left(\frac{1}{2}\sigma_{z,i}\cdot\varepsilon_i(V, d) + \frac{1}{2}\sigma_{x,i}\cdot\Delta_i(d) \right) + \frac{1}{2}g\sigma_{z,A}\sigma_{z,B} \tag{1}$$

where σ is the Pauli operator for a TLS of H_2, ε_i (V, d) is the energy spacing of the two levels that depends on sample bias V and tip−surface separation d, and $\Delta_i(d)$ represents the tunnel coupling between the two levels, which is inversely related to d,[12] as schematically shown in Figure 2(b,c). The double-well potential that H_2 experiences should be formed through the van der Waals forces exerted by both the tip and the surface, where the two local minima correspond to H_2 interacting more with the tip or the surface.[38] Further discussion of the spectral evidence for the nature of two levels of H_2 is given in Section S4 of the Support Information (SI). When the tip is brought closer to the surface, the energy barrier between the two wells is suppressed, resulting in a larger $\Delta(d)$. The strength of the dipolar interaction, denoted by g, comprises the strain-mediated elastic interaction as well as an electric dipole interaction contribution. By calculating the eigenstates and their eigenenergies, we provide a typical single-excitation spectrum of this two-body system in Figure 2(d,e) to illustrate the avoided level crossing. The interaction can introduce a gap when the resonance frequencies of two H_2 molecules are close to each other, and the size of the gap is

$$g_\perp = g\frac{\Delta_A(d)\Delta_B(d)}{E^2} \tag{2}$$

where E is the energy of the gap center. The $g_\parallel$ in Figure 2(d) defines the size of distortion near the tuning point of the TLS of either one of the H_2 molecules. Additional details about the model can be found in Section S1 of the Supporting Information. By fixing the sample bias at −5 mV around the level crossing region and tuning the size of the junction, we found the gap shown in Figure 2(f) increased, as anticipated due to the corresponding increase in $\Delta(d)$. By employing this model, we could fit the data of Figure 1(f–h) as shown in Figure 3. The resulting physical quantities have been derived and are presented in Table S1 of the SI.

Bias Dependence of Signal Strength. The oscillation amplitude of the THz-induced DC current is proportional to the disparity in conductance between excited and ground states of the H_2 molecule being measured. Each eigenstate is a superposition of the two adsorption configurations of H_2 within the junction and with distinct conductance, as verified by the telegraph noise (switching between two current levels) of the junction conductance. Therefore, it can be inferred that the signal strength is directly proportional to the absolute value

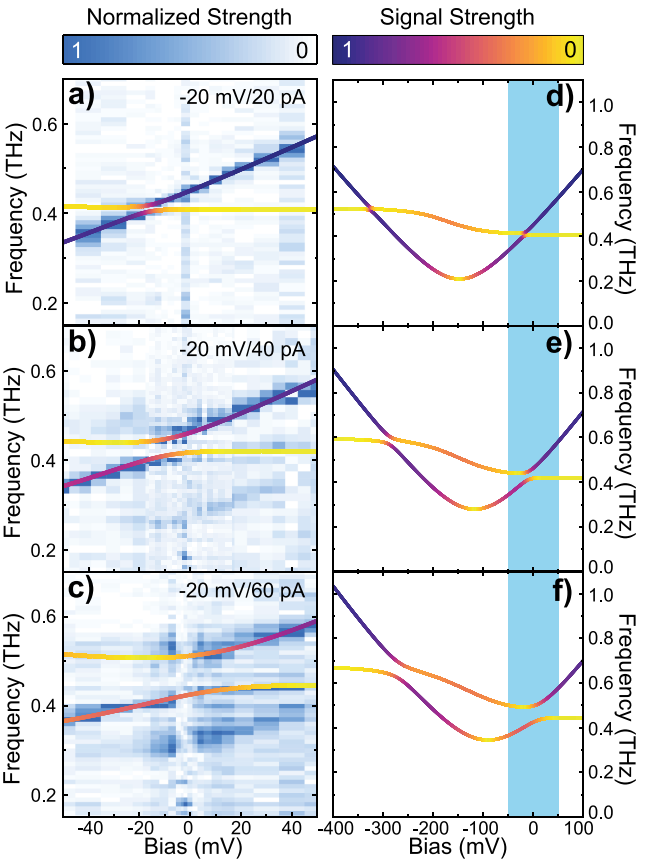

Figure 3. Avoided level crossing from the interaction of two H_2 molecules. (a–c) Bias dependence of resonance frequency of a H_2 that is coherently coupled to a second H_2 with decreasing size of the junction controlled by the set point [(a) −20 mV/20 pA; (b) −20 mV/40 pA; (c) −20 mV/60 pA]. The fitting results were superimposed on the data with the color specifying the calculated signal strength for the two H_2 molecules. (d)–(f) are the extrapolated fitting results of (a)–(c) with a large bias range to illustrate the overall excitation spectrum of the two H_2 molecules. The blue-shaded strip indicates the bias range covered by the experimental results.

of the population change of either adsorption configuration for the H_2 being measured, as detailed in Section S2 of the SI.

$$S(\omega_m) = S\left(\frac{\tilde{E}_m - \tilde{E}_g}{\hbar}\right) \propto |P_{R_A,m} - P_{R_A,g}| = |P_{L_A,m} - P_{L_A,g}| \tag{3}$$

Here, $\tilde{E}_m$ and $\tilde{E}_g$ are the eigenenergies of the excited state $|m\rangle$ and ground state $|g\rangle$, and $\omega_m = (\tilde{E}_m - \tilde{E}_g)/\hbar$ is the corresponding oscillation frequency. P is the population of either configuration ($|L\rangle$ or $|R\rangle$) of the H_2, and the subscript A specifies the H_2 that is mainly measured or responsible for the tunneling current. There are three excited states that we modeled, as shown in Figure S2 of the SI. However, the one with the highest energy corresponds to a two-photon absorption process, which can be neglected for its low excitation probability. Based on eq 3, we denoted the predicted signal strength through the colors for the two excited states on the calculated curves shown in Figure 2(d,e) and Figure 3. The nearly yellow branch in Figure 2(d), representing the excitation spectrum of the other H_2, was barely observed at most biases. This is attributed to the fact that only a few H_2

https://doi.org/10.1021/acsnano.3c09109
ACS Nano 2023, 17, 23144−23151

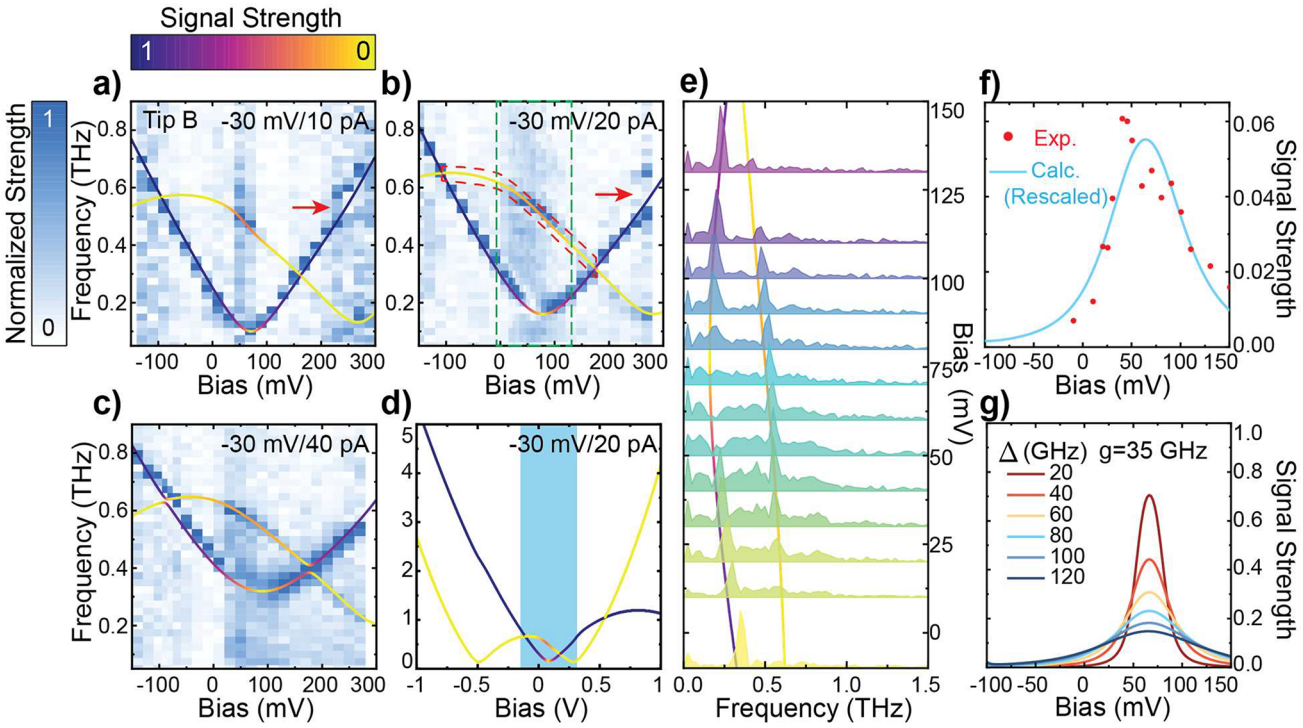

Figure 4. Entanglement between two H_2 molecules. (a−c) Bias dependence of the resonance frequency of H_2 in the tunneling junction that is coherently coupled to a second H_2 with decreasing size of the junction controlled by the set point [(a) −30 mV/10 pA; (b) −30 mV/20 pA; (c) −30 mV/40 pA] for a different tip (tip B). The experimental data were adopted from Figure 3 in ref 29. The fitting results were superimposed on the data with the color specifying the calculated signal strength from the model. (d) Calculated excitation spectrum of (b) for a large bias range (−1000 to 1000 mV). The shaded area corresponds to the bias range shown in (b). (e) FFT spectra before normalization in the bias range of −10 to 130 mV as indicated by the green dashed box in (b) but plotted by stacking them with separation scaled to the sample bias. (f) A comparison between the experimental signal strength of the branch encircled by a red dashed box in (b) and the corresponding calculated results. The experimental values were picked from the corresponding peak of FFT spectra. (g) Calculated signal strength of the curve in the same bias range as (f), but for different tunneling coupling Δ (20−120 GHz). Other parameters were set the same as the fitting curves in (b) and (f).

molecules can exist within the limited space of the junction and be sensed through the measurement of THz-induced DC current. The H_2 (the H_2 molecule B, $H_{2,B}$) that happens to have the same resonance frequency and be resonant with the H_2 in the junction (the H_2 molecule A, $H_{2,A}$) could be outside the junction and has a minor influence on the junction conductance. Nevertheless, we noticed from the extrapolated spectra in Figure 3(d−f) that there is a certain region of the branch for H_2 molecule B between the two crossing points that shows an appreciable signal. This seems to imply that the information on the H_2 outside of the junction can be obtained through the projective measurements on the H_2 in the junction due to the formation of the entangled states for the two interacting H_2 molecules.

We indeed found this entanglement with a different tip[29] which exhibited H_2 oscillation for a larger range of bias in Figure 4(a−c) at various tip−sample separations. Only a portion of the yellow branch belonging to the H_2 outside of the junction displayed a signal, while the signal on another branch vanished at the corresponding biases. The change of signal strength of two branches with respect to the bias can be explained by eq 3 as the mixing degree of two H_2 molecules varies with bias. Further analysis is available in Sections S2 and S3 of the SI. Both the frequency shift and signal strength were well fitted given the parameters listed in Table S1. Figure 4(d) shows the extrapolated excitation spectrum for Figure 4(b) and provides an overview of the energy landscape. The fast Fourier transform (FFT) spectrum at each bias in Figure 4(a−c) was normalized for a better visibility, which might lead to the artifact of the signal variation at a certain region. To address this, we examined, in Figure 4(e), the unnormalized FFT spectra of Figure 4(b), where the bias range is indicated by a dashed green box. A clear peak emerges for the branch with higher energy at the biases close to the tuning point of the lower parabola, and the extracted peak height follows the trend of the calculated result as shown in Figure 4(f). In addition, we have included the unnormalized data of Figure 4(a−c) across the entire bias range in Figure S7 of the SI to remove any normalization artifacts. The visible range of the excitation signal for the branch with higher energy broadens when the tip gets closer to the surface, as shown in Figure 4(a−c). This broadening could be attributed to the increasing tunnel coupling, as supported by the calculation in Figure 4(g). Furthermore, the tunnel coupling for the TLS of H_2 could be modified by moving the tip to different sites of the Cu_2N island due to chemical inhomogeneity of the surface. This, in turn, could affect the visible range of the upper branch, as demonstrated in Figure S5 of the SI.

It is noteworthy that a similar model has been applied to elucidate the interplay among multiple TLSs present in amorphous materials, particularly in experiments involving superconducting devices where the model was employed to analyze the distortion of the excitation spectrum for the interacting TLSs.[8,37] In our experiments, H_2 molecules do not

https://doi.org/10.1021/acsnano.3c09109
ACS Nano 2023, 17, 23144−23151

contribute equally to the measured THz-induced DC signal, and therefore the entangled property between these two quantum entities is highlighted.

Multiple Interacting TLSs. So far, only the interaction between the two H_2 molecules has been discussed. However, multiple H_2 molecules that are in proximity to the junction are expected to interact with the junction H_2 that dominates the measured signal. The energy differences of the TLSs for these H_2 molecules are likely to vary from each other, as they are subjected to different local environments. Although their conductance switching might not be sensed by the tunneling current, the H_2 molecules could still resonate with junction H_2 when they share the same excitation energy by tuning the sample bias. For example, the gaps indicated by the red arrows in Figure 4(a) and (b) suggest the existence of a third H_2. With a different tip, multiple avoided level crossings could be observed on the Stark shift of the H_2 in the junction as shown in Figure 5. A similar phenomenon has been observed and extensively studied in superconducting devices.[5,7,39] The junction H_2 in our work performed the equivalent of the phase qubit in superconducting devices, and the resonance frequency can be directly read out. The other H_2 molecules on the surface play the role of multiple atomic TLSs that reside in the insulation layer of the Josephson junction. However, due to a lack of independent tunable parameters and finite size of the tunnel junction, we were unable to simultaneously observe the energy evolution of all the TLSs, unlike what was demonstrated in the superconducting devices.[7,10,11,40] Nevertheless, by altering the tip−sample separation and monitoring the gaps at different frequencies, as shown in Figure S8 of the SI, we can still observe the energy evolution of the H_2 outside of the junction at a distance on the order of the size of the junction.

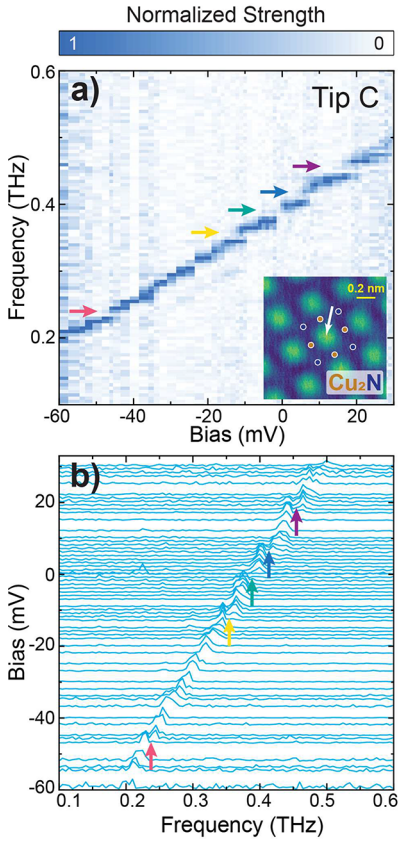

Figure 5. Interactions among multiple H_2 molecules in the junction. (a) The bias dependence of the H_2 resonance frequency for a third tip (tip C). The tip height was set by the set point of −20 mV/40 pA. The avoided level crossing gaps are indicated by the arrows. The inset is a topography of the Cu_2N island imaged by this tip under the set point of −20 mV/40 pA, with the arrow indicating tip position where the data were taken. (b) The same results as (a) but shown from a different perspective and plotted by directly stacking the normalized FFT spectra for different biases indicated by the position of the baselines. The counterpart of avoided level crossing gaps of (a) are also illustrated by arrows with corresponding colors.

CONCLUSIONS

In conclusion, we proposed a direct dipolar-type interaction of 20−200 GHz among the TLSs of physisorbed H_2 molecules to explain the avoided level crossing and variation of signal strength observed from the energy evolution for the TLSs of H_2 in the STM cavity with respect to the electric field. The implications of introducing such an interaction in this work could be significant for those seeking H_2 storage materials.[41] Furthermore, dipolar interactions between H_2 and other quantum materials, like heterostructures of 2D materials, should also be anticipated. Therefore, a H_2-based dipole sensor would facilitate the study of dipole-related properties for those materials.[42−46] However, clarifying the nature of the interaction is apparently a challenge of DFT calculations owing to the small energy differences between configurations and the zero-point motion of the protons. Results obtained in this work should stimulate further development in experiment and theory of the coherence of two-level systems.

METHODS

The experiments were performed in a home-built ultra-high-vacuum STM operating at 9.0 K with electrochemically etched silver tips. The Cu(001) surface was cleaned by Ne^+ sputtering and annealing at 790 K. A single atomic layer of Cu_2N was prepared by sputtering the clean Cu(001) surface with an ionized N_2 beam and annealing to 630 K. Hydrogen molecules in the background of the ultra-high-vacuum chamber preferentially adsorbed on the Cu_2N islands and could be completely desorbed by 820 nm laser illumination.

A femtosecond Ti:sapphire laser with a 1 GHz repetition rate (Laser Quantum Taccor Ultra 8) was used to generate THz pulses from a plasmonic photoconductive antenna (PCA) fabricated by Mona Jarrahi's group at UCLA.[47] The THz pulses with linear polarization were aligned and focused into the tunnel junction through flat silver mirrors and an aspheric Tsurupica lens. More details on the optical setup can be found in previous work.[27]

The STM topographic images were plane fitted to correct for the slight sample slope. For IETS measurements, the lock-in amplifier was used in the internal reference mode with a sinusoidal modulation frequency of 263.03 Hz and amplitude of 3 mV to record simultaneously the first and second harmonic signals. For TIDCS and delay-scan spectra, a square wave of 263.03 Hz from the lock-in amplifier was externally amplified and used to modulate the PCA to chop the THz pulses. The THz-induced current was detected by measuring the first harmonic signal of the lock-in amplifier as a difference in the DC between the THz-on period and the THz-off period of the square wave modulation.

ASSOCIATED CONTENT

Supporting Information

The Supporting Information is available free of charge at https://pubs.acs.org/doi/10.1021/acsnano.3c09109.

https://doi.org/10.1021/acsnano.3c09109
ACS Nano 2023, 17, 23144−23151

Detailed analysis on the Hamiltonian; calculation of signal strength at the detected resonance frequencies; supplementary data for tip B; parameters of fitting for figures in the article; multiple avoided level crossing observed with a fourth tip (tip D); discussion on the physics nature of TLS for a H_2 molecule in the junction (PDF)

AUTHOR INFORMATION

Corresponding Author

Wilson Ho − *Department of Physics and Astronomy, University of California, Irvine, California 92697-4575, United States; Department of Chemistry, University of California, Irvine, California 92697-2025, United States;* orcid.org/0000-0003-3884-2142; Email: wilsonho@uci.edu

Authors

Yunpeng Xia − *Department of Physics and Astronomy, University of California, Irvine, California 92697-4575, United States;* orcid.org/0000-0001-5750-809X

Likun Wang − *Department of Physics and Astronomy, University of California, Irvine, California 92697-4575, United States;* orcid.org/0000-0002-4082-9548

Dan Bai − *Department of Physics and Astronomy, University of California, Irvine, California 92697-4575, United States;* orcid.org/0000-0002-7588-490X

Complete contact information is available at: https://pubs.acs.org/10.1021/acsnano.3c09109

Funding

This work was supported by the U.S. Department of Energy, Office of Basic Energy Sciences, awards DE-SC0019448 and DE-SC0024037. In addition, we gratefully acknowledge a Fellowship to Y.X. by the Eddleman Quantum Institute at UCI. The plasmonic photoconductive antenna was fabricated by M. Jarrahi's group at the University of California, Los Angeles.

Notes

The authors declare no competing financial interest.

ABBREVIATIONS

STM, scanning tunneling microscope; TLS, two-level system; QSM, quantum superposition microscope; IETS, inelastic electron tunneling spectroscopy; TIDCS, THz-induced direct current spectroscopy; FFT, fast Fourier transform; PCA, plasmonic photoconductive antenna

REFERENCES

(1) Phillips, W. A. Two-Level States in Glasses. *Rep. Prog. Phys.* **1987**, *50*, 1657.

(2) Yu, C. C.; Leggett, A. J. Low Temperature Properties of Amorphous Materials: Through a Glass Darkly. *Comments Cond. Mater. Phys.* **1988**, *14*, 231−251.

(3) Yu, C. C. Interacting Defect Model of Glasses: Why Do Phonons Go So Far? *Phys. Rev. Lett.* **1989**, *63*, 1160−1163.

(4) Carruzzo, H. M.; Yu, C. C. Why Phonon Scattering in Glasses is Universally Small at Low Temperatures. *Phys. Rev. Lett.* **2020**, *124*, 075902.

(5) Simmonds, R. W.; Lang, K. M.; Hite, D. A.; Nam, S.; Pappas, D. P.; Martinis, J. M. Decoherence in Josephson Phase Qubits from Junction Resonators. *Phys. Rev. Lett.* **2004**, *93*, 077003.

(6) Martinis, J. M.; Cooper, K. B.; McDermott, R.; Steffen, M.; Ansmann, M.; Osborn, K. D.; Cicak, K.; Oh, S.; Pappas, D. P.; Simmonds, R. W.; Yu, C. C. Decoherence in Josephson Qubits from Dielectric Loss. *Phys. Rev. Lett.* **2005**, *95*, 210503.

(7) Grabovskij, G. J.; Peichl, T.; Lisenfeld, J.; Weiss, G.; Ustinov, A. V. Strain Tuning of Individual Atomic Tunneling Systems Detected by a Superconducting Qubit. *Science* **2012**, *338*, 232−234.

(8) Lisenfeld, J.; Grabovskij, G. J.; Müller, C.; Cole, J. H.; Weiss, G.; Ustinov, A. V. Observation of Directly Interacting Coherent Two-Level Systems in an Amorphous Material. *Nat. Commun.* **2015**, *6*, 6182.

(9) Sarabi, B.; Ramanayaka, A. N.; Burin, A. L.; Wellstood, F. C.; Osborn, K. D. Projected Dipole Moments of Individual Two-Level Defects Extracted Using Circuit Quantum Electrodynamics. *Phys. Rev. Lett.* **2016**, *116*, 167002.

(10) Lisenfeld, J.; Bilmes, A.; Matityahu, S.; Zanker, S.; Marthaler, M.; Schechter, M.; Schön, G.; Shnirman, A.; Weiss, G.; Ustinov, A. V. Decoherence Spectroscopy with Individual Two-Level Tunneling Defects. *Sci. Rep.* **2016**, *6*, 23786.

(11) Lisenfeld, J.; Bilmes, A.; Megrant, A.; Barends, R.; Kelly, J.; Klimov, P.; Weiss, G.; Martinis, J. M.; Ustinov, A. V. Electric Field Spectroscopy of Material Defects in Transmon Qubits. *npj Quantum Inf.* **2019**, *5*, 105.

(12) Müller, C.; Cole, J. H.; Lisenfeld, J. Towards Understanding Two-Level-Systems in Amorphous Solids: Insights from Quantum Circuits. *Rep. Prog. Phys.* **2019**, *82*, 124501.

(13) Gupta, J. A.; Lutz, C. P.; Heinrich, A. J.; Eigler, D. M. Strongly Coverage-Dependent Excitations of adsorbed molecular hydrogen. *Phys. Rev. B* **2005**, *71*, 115416.

(14) Lotze, C.; Corso, M.; Franke, K. J.; Von Oppen, F.; Pascual, J. I. Driving a Macroscopic Oscillator with the Stochastic Motion of a Hydrogen Molecule. *Science* **2012**, *338*, 779−782.

(15) Jung, J.; Nam, S.; Wolf, C.; Heinrich, A. J.; Chae, J. Atomic-Scale Intermolecular Interaction of Hydrogen with a Single VOPc Molecule on the Au(111) Surface. *RSC Adv.* **2021**, *11*, 6240−6245.

(16) Thijssen, W. H. A.; Djukic, D.; Otte, A. F.; Bremmer, R. H.; Van Ruitenbeek, J. M. Vibrationally Induced Two-Level Systems in Single-Molecule Junctions. *Phys. Rev. Lett.* **2006**, *97*, 226806.

(17) Halbritter, A.; Makk, P.; Csonka, S.; Mihály, G. Huge Negative Differential Conductance in Au−H_2 Molecular Nanojunctions. *Phys. Rev. B* **2008**, *77*, 075402.

(18) Nielsen, M. Phonons in Solid Hydrogen and Deuterium Studied by Inelastic Coherent Neutron Scattering. *Phys. Rev. B* **1973**, *7*, 1626−1635.

(19) Natterer, F. D.; Patthey, F.; Brune, H. Resonant-Enhanced Spectroscopy of Molecular Rotations with a Scanning Tunneling Microscope. *ACS Nano* **2014**, *8*, 7099−7105.

(20) Therrien, A. J.; Pronschinske, A.; Murphy, C. J.; Lewis, E. A.; Liriano, M. L.; Marcinkowski, M. D.; Sykes, E. C. H. Collective Effects in Physisorbed Molecular Hydrogen on Ni/Au(111). *Phys. Rev. B* **2015**, *92*, 161407.

(21) Cocker, T. L.; Jelic, V.; Gupta, M.; Molesky, S. J.; Burgess, J. A. J.; Reyes, G. D. L.; Titova, L. V.; Tsui, Y. Y.; Freeman, M. R.; Hegmann, F. A. An Ultrafast Terahertz Scanning Tunnelling Microscope. *Nat. Photonics* **2013**, *7*, 620−625.

(22) Cocker, T. L.; Peller, D.; Yu, P.; Repp, J.; Huber, R. Tracking the Ultrafast Motion of a Single Molecule by Femtosecond Orbital Imaging. *Nature* **2016**, *539*, 263−267.

(23) Jelic, V.; Iwaszczuk, K.; Nguyen, P. H.; Rathje, C.; Hornig, G. J.; Sharum, H. M.; Hoffman, J. R.; Freeman, M. R.; Hegmann, F. A. Ultrafast Terahertz Control of Extreme Tunnel Currents through Single Atoms on a Silicon Surface. *Nat. Physics* **2017**, *13*, 591−598.

(24) Yoshida, S.; Arashida, Y.; Hirori, H.; Tachizaki, T.; Taninaka, A.; Ueno, H.; Takeuchi, O.; Shigekawa, H. Terahertz Scanning Tunneling Microscopy for Visualizing Ultrafast Electron Motion in Nanoscale Potential Variations. *ACS Photonics* **2021**, *8*, 315−323.

(25) Müller, M.; Martín Sabanés, N.; Kampfrath, T.; Wolf, M. Phase-Resolved Detection of Ultrabroadband THz Pulses inside a

Scanning Tunneling Microscope Junction. *ACS Photonics* **2020**, *7*, 2046−2055.
(26) Peller, D.; Roelcke, C.; Kastner, L. Z.; Buchner, T.; Neef, A.; Hayes, J.; Bonafé, F.; Sidler, D.; Ruggenthaler, M.; Rubio, A.; Huber, R.; Repp, J. Quantitative Sampling of Atomic-Scale Electromagnetic Waveforms. *Nat. Photonics* **2021**, *15*, 143−147.
(27) Wang, L.; Xia, Y.; Ho, W. Atomic-Scale Quantum Sensing Based on the Ultrafast Coherence of an H_2 Molecule in an STM Cavity. *Science* **2022**, *376*, 401−405.
(28) Sheng, S.; Oeter, A.-C.; Abdo, M.; Lichtenberg, K.; Hentschel, M.; Loth, S. Launching Coherent Acoustic Phonon Wave Packets with Local Femtosecond Coulomb Forces. *Phys. Rev. Lett.* **2022**, *129*, 043001.
(29) Wang, L.; Bai, D.; Xia, Y.; Ho, W. Electrical Manipulation of Quantum Coherence in a Two-Level Molecular System. *Phys. Rev. Lett.* **2023**, *130*, 096201.
(30) Li, S.; Yu, A.; Toledo, F.; Han, Z.; Wang, H.; He, H. Y.; Wu, R.; Ho, W. Rotational and Vibrational Excitations of a Hydrogen Molecule Trapped within a Nanocavity of Tunable Dimension. *Phys. Rev. Lett.* **2013**, *111*, 146102.
(31) Natterer, F. D.; Patthey, F.; Brune, H. Distinction of Nuclear Spin States with the Scanning Tunneling Microscope. *Phys. Rev. Lett.* **2013**, *111*, 175303.
(32) Jaynes, E. T.; Cummings, F. W. Comparison of Quantum and Semiclassical Radiation Theories with Application to the Beam Maser. *Proc. IEEE* **1963**, *51*, 89−109.
(33) Dong, Z. C.; Zhang, X. L.; Gao, H. Y.; Luo, Y.; Zhang, C.; Chen, L. G.; Zhang, R.; Tao, X.; Zhang, Y.; Yang, J. L.; Hou, J. G. Generation of Molecular Hot Electroluminescence by Resonant Nanocavity Plasmons. *Nat. Photonics* **2010**, *4*, 50−54.
(34) Joffrin, J.; Levelut, A. Virtual Phonon Exchange in Glasses. *J. Phys. (Paris)* **1975**, *36*, 811−822.
(35) Klein, M. W.; Fischer, B.; Anderson, A.; Anthony, P. Strain Interactions and the Low-Temperature Properties of Glasses. *Phys. Rev. B* **1978**, *18*, 5887.
(36) Svensson, K.; Andersson, S. Dipole Active Vibrational Motion in the Physisorption Well. *Phys. Rev. Lett.* **1997**, *78*, 2016−2019.
(37) de los Santos-Sánchez, O.; Román-Ancheyta, R. Strain-Spectroscopy of Strongly Interacting Defects in Superconducting Qubits. *Supercond. Sci. Technol.* **2022**, *35*, 035005.
(38) Weiss, C.; Wagner, C.; Kleimann, C.; Rohlfing, M.; Tautz, F. S.; Temirov, R. Imaging Pauli Repulsion in Scanning Tunneling Microscopy. *Phys. Rev. Lett.* **2010**, *105*, 086103.
(39) Palomaki, T. A.; Dutta, S. K.; Lewis, R. M.; Przybysz, A. J.; Paik, H.; Cooper, B. K.; Kwon, H.; Anderson, J. R.; Lobb, C. J.; Wellstood, F. C.; Tiesinga, E. Multilevel Spectroscopy of Two-Level Systems Coupled to a dc SQUID Phase Qubit. *Phys. Rev. B* **2010**, *81*, 144503.
(40) Bilmes, A.; Volosheniuk, S.; Brehm, J. D.; Ustinov, A. V.; Lisenfeld, J. Quantum Sensors for Microscopic Tunneling Systems. *npj Quantum Inf.* **2021**, *7*, 27.
(41) Nijkamp, M.; Raaymakers, J.; Van Dillen, A.; De Jong, K. Hydrogen Storage Using Physisorption−Materials Demands. *Appl. Phys. A: Mater. Sci. Process.* **2001**, *72*, 619−623.
(42) Unuchek, D.; Ciarrocchi, A.; Avsar, A.; Watanabe, K.; Taniguchi, T.; Kis, A. Room-Temperature Electrical Control of Exciton Flux in a Van Der Waals Heterostructure. *Nature* **2018**, *560*, 340−344.
(43) Ciarrocchi, A.; Unuchek, D.; Avsar, A.; Watanabe, K.; Taniguchi, T.; Kis, A. Polarization Switching and Electrical Control of Interlayer Excitons in Two-Dimensional Van Der Waals Heterostructures. *Nat. Photonics* **2019**, *13*, 131−136.
(44) Li, W.; Lu, X.; Dubey, S.; Devenica, L.; Srivastava, A. Dipolar Interactions Between Localized Interlayer Excitons in Van Der Waals Heterostructures. *Nat. Mater.* **2020**, *19*, 624−629.
(45) Chen, Y.; Liu, Z.; Li, J.; Cheng, X.; Ma, J.; Wang, H.; Li, D. Robust Interlayer Coupling in Two-Dimensional Perovskite/Monolayer Transition Metal Dichalcogenide Heterostructures. *ACS Nano* **2020**, *14*, 10258−10264.
(46) Chiodini, S.; Kerfoot, J.; Venturi, G.; Mignuzzi, S.; Alexeev, E. M.; Teixeira Rosa, B. r.; Tongay, S.; Taniguchi, T.; Watanabe, K.; Ferrari, A. C. Moiré Modulation of Van Der Waals Potential in Twisted Hexagonal Boron Nitride. *ACS Nano* **2022**, *16*, 7589−7604.
(47) Yardimci, N. T.; Yang, S. H.; Berry, C. W.; Jarrahi, M. High-Power Terahertz Generation Using Large-Area Plasmonic Photoconductive Emitters. *IEEE Trans. Terahertz Sci. and Technol.* **2015**, *5*, 223−229.

https://doi.org/10.1021/acsnano.3c09109
ACS Nano 2023, 17, 23144−23151